# Detection of Esterified Cholesterol in Murine Bruch's Membrane Wholemounts With a Perfringolysin O-Based Cholesterol Marker

Martin Rudolf,[1] Armin Mohi,[1] Marie C. Dettbarn,[1] Yoko Miura,[1] Zouhair Aherrahrou,[2] Mahdy Ranjbar,[1] Bulent Mutus,[3] and Johannes K. M. Knobloch[4]

[1]Department of Ophthalmology, University of Lübeck, Lübeck, Germany
[2]Institute for Integrative and Experimental Genomics, University of Lübeck, Lübeck, Germany
[3]Department of Chemistry & Biochemistry, University of Windsor, Windsor, Ontario, Canada
[4]Institute for Medical Microbiology & Hygiene, University of Lübeck, Lübeck, Germany

Correspondence: Martin Rudolf, University Eye Hospital Lübeck, University of Lübeck, Ratzeburger Allee 160, 23538 Lübeck, Germany; mirudolf@aol.com.

MRu, AM and BM, JKMK contributed equally to the work presented here and should therefore be regarded as equivalent authors.

Submitted: March 6, 2014
Accepted: May 22, 2014

Citation: Rudolf M, Mohi A, Dettbarn MC, et al. Detection of esterified cholesterol in murine Bruch's membrane wholemounts with a perfringolysin O-based cholesterol marker. *Invest Ophthalmol Vis Sci*. 2014;55:4759–4767. DOI:10.1167/iovs.14-14311

**Purpose.** To investigate the effects of Bruch's membrane (BrM) neutral lipid deposition in mouse models and its significance to aging and age-related macular degeneration, it is essential to reliably detect small quantities of neutral lipids including esterified cholesterol (EC). In chorioretinal sections and BrM wholemounts, we tested a novel fluorescent cholesterol marker based on the bacterial toxin perfringolysin O (PFO) and compared results with those obtained with the classic cholesterol dye filipin.

**Methods.** An engineered plasmid containing the specific cholesterol binding domain (D4) of PFO fused to green fluorescent protein (GFP) was expressed in cultured *E. coli*, isolated, purified, and concentrated. A total of 150 BrM-choroid wholemounts and chorioretinal sections of 11- to 13-month-old ApoE$^{null}$ mice were prepared and stained with PFO/D4-GFP or filipin for EC. Samples were examined by epifluorescence microscopy.

**Results.** The fluorescence intensity of PFO/D4-GFP was strong, stable, and, if small quantities of EC were present, superior to filipin. In all specimens, we could sharply locate the PFO/D4-GFP signal to BrM. A semiquantitative evaluation of BrM lipid deposition is possible by measuring PFO/D4-GFP fluorescence intensity.

**Conclusions.** The use of PFO/D4-GFP allowed a robust and direct detection of EC in aged murine BrM. In wholemount samples, its strong and stable fluorescence facilitated a semiquantitative evaluation of BrM-EC content over a large area. The patterns of EC deposition in murine BrM wholemounts are comparable with findings in human BrM wholemounts. Perfringolysin O/D4-GFP could be an important tool for investigating the effects of BrM lipid deposition in mouse models.

Keywords: Bruch's membrane, lipids, aging, mouse model, cholesterol marker

Cholesterol is a multifunctional lipid and is universally present in most eukaryotic cell membranes. Its esterified form is a major neutral lipid and is exclusively used for intracellular storage and for systemic lipid transport via lipoproteins. Pathological lipid accumulation is a key mechanism in several diseases like atherosclerosis, age-related macular degeneration, and Niemann-Pick syndrome.[1–3] The polyene macrolide antibiotic filipin is today the only commercially available marker, which binds specifically to the 3β-hydroxyl group of unesterified cholesterol and exhibits fluorescent activity if stimulated by light at short wavelengths (excitation: 340–380 nm, emission: 385–470 nm).[4–6] Nevertheless, filipin fluorescence fades fast, making the reliable detection of especially small cholesterol quantities difficult.[3,7]

Pathological relevant neutral lipid accumulations in Bruch's membrane (BrM) and in deposits underneath the RPE like drusen and basal deposits are of high interest in AMD research.[2] The basis of these lipid deposits are RPE-derived lipoproteins that are highly enriched in esterified cholesterol (EC).[2,8,9] It was already shown that EC is highly specific for these extracellular lesions.[9,10] In aged and thickened human BrMs (2–5 μm), EC is abundantly present and can be easily visualized by filipin in chorioretinal sections and in wholemount preparations.[5,10,11] However, EC is not directly detectable by filipin. A protocol is used where unesterified cholesterol is extracted by 70% ethanol. The remaining EC is then hydrolyzed by a cholesterol esterase to set unesterified cholesterol free, which is again specifically detectable by filipin.

Mouse models are frequently used to investigate biological effects of these lipid accumulations on BrM itself and its adjacent structures like choriocapillaris, the RPE, and neuroretina.[12–15] Murine BrM is much thinner (300–500 nm) than its human correspondent and if aged, it is thickened up to 1.2 μm.[16] The total amount of age-related lipid rich deposits is accordantly less. Neutral lipids in aged murine BrM are in general also vaguely detectable by the classic neutral lipid stain oil red O and EC with filipin.[12,15] But these staining methods are not strong enough for a reliable systematic semiquantitative evaluation. Oil red O is nonfluorescent and stains BrM in chorioretinal sections only patchy.[15] Filipin exhibits in small

quantities only a low fluorescence and fades too fast for valid photo documentation. Lipid detection in murine BrM wholemounts is not possible with these techniques.

For this reason, transmission electron microscopy (TEM) is considered the gold standard in murine models of age-related lipid deposition.[13,14,16] The structure of BrM and the adjacent structures can be easily evaluated. But this technique has several limitations. It is time intensive and allows us to analyze only a small BrM section at a time. Another big drawback is that during normal tissue processing for TEM, all lipids are washed out, which leaves empty lipid-derived vacuoles behind. This allows only an indirect structural evaluation of the degree of lipid accumulation.[16]

Our aim was to establish a quick, reliable, and direct detection method to evaluate EC in murine BrM over a large area. For this purpose, we needed a highly specific cholesterol dye with strong and stable fluorescence that works in murine wholemount preparations. A new approach is the use of specific cholesterol binding bacterial toxins like perfringolysin O (PFO) secreted by the bacterium *Clostridium perfringens*.[7,17,18] Perfringolysin O belongs to a large family of membrane pore–forming toxins called cholesterol-dependent cytolysins that are secreted by different Gram-positive bacteria.[17] The recognition of unesterified cholesterol is realized by PFOs nontoxic domain 4 (PFO/D4).[19] An analog to filipin, EC can only be indirectly detected by PFO/D4 after unesterified cholesterol is set free by EC hydrolysis. In this study, we used an engineered plasmid to express PFO/D4 bound to green fluorescent protein (GFP) as a highly specific cholesterol marker.[20] To our knowledge, we are the first to use a cytolysin-based cholesterol marker for histochemistry in the eye. We describe a protocol for reliable EC detection in murine BrM and staining pattern, important to a semiquantitative analysis approach of BrM EC content.

## Methods

In an initial feasibility study, we compared the cholesterol markers PFO/D4-GFP and filipin for EC detection in BrM wholemounts and chorioretinal sections of aged $ApoE^{null}$ mice. We checked for the influence of a high-cholesterol diet and verified the presence of lipid accumulation in BrM with electron microscopy. In a follow-up study, we evaluated the reproducibility of our new staining method for EC in murine BrM wholemounts and analyzed factors influencing a systematic evaluation of BrM lipid content.

### Mouse Model

Female homozygous $ApoE^{null}$ mice with a C57BL/6J background were purchased from Jackson Laboratories (B6.129P2-Apoetm1Unc/J; Bar Harbor, ME, USA). These animals are a classic atherosclerosis mouse model with genetic hypercholesterolemia and extensive lipid deposits in BrM with age.[13] Animals were handled in accordance with the ARVO Statement for the Use of Animals in Ophthalmic and Vision Research. Ethics committee approval was obtained. Animals were kept in plastic cages with regular light-dark cycles and had continuous free access to water and food. All animals received a regular rodent chow diet (Altromin 1324-pellet; Altromin, Lage, Germany).

In the feasibility study we used 11-month-old mice fed only with regular chow ($n = 10$) and 9- to 10-month-old mice with a high cholesterol diet ($n = 10$, TD 92121; Teklad Custom Research Diets, Madison, WI, USA) for 6 weeks. For comparison, we used young 3-month-old mice on chow feeding. In our follow-up study we used only aged mice (11–13 months old, $n = 60$) on regular chow feeding.

### Tissue Harvesting and Preparation

At the age of 11 to 13 months, all mice were weighted and then killed by thoracotomy and opening of the left cardiac ventricle for exsanguination in deep isofluorane anesthesia. During exsanguination, the mice were perfused with 1.25% paraformaldehyde (PFA)/0.8% glutaraldehyde in 0.1 M Sorensen buffer via the left cardiac ventricle for prompt tissue fixation and elimination of remaining intravascular blood including serum lipids, which is an important source of background artefacts in stained wholemount preparations. The eyes were enucleated and immediately processed.

In our feasibility study, one eye per mouse was immediately prepared as BrM-choroid-sclera wholemount. First, we removed the anterior segment including the lens under a stereomicroscope (Leica M125; Leica Microsystems, Wetzlar, Germany). The remaining globe was cut radially several times and the retina was completely removed with a fine tip forceps. The RPE was gently brushed off with fine art brushes. Finally, the wholemounts were placed in the above mentioned fixative for 3 days at 4°C and was then moved to 1% PFA at 4°C for storage until staining. Random samples were taken from a few wholemounts for preparation quality control. These specimens were cryoembedded (see below for procedure) and sectioned to BrM-choroid samples without RPE and retina.

Five eyes per group were prepared for electron microscopy. After storage in the perfusion fixative at 4°C for 3 days, eyes were postfixed in 2% buffered osmium tetroxide, dehydrated in a graded ethanol series, and embedded in epoxy resin (PolyBed 812; Polysciences, Warrington, PA, USA) according to standard protocols. Sections 1-μm thick were cut (Ultracut UCT/EM/FCS; Leica Microsystems). Counterstaining with uranyl acetate or lead citrate was not necessary.

The remaining five eyes per group were prepared for cryoembedding after running through a sucrose/embedding medium (Tissue-Tek OCT Compound; Sakura, AJ Alphen aan den Rij, The Netherlands) series as described before.[21] The eyes were placed in cryomolds in a final mixture of 2:1 and were stored at −80°C. Eight-millimeter-thick cryosections were cut with a microtome (CM 3050 S; Leica Microsystems), placed on slides, and stored at −20°C until staining.

In our follow-up study, we prepared 120 wholemounts as described above. All together, we stained and evaluated a total of 150 BrM wholemounts.

### PFO/D4-GFP Plasmid Expression and Protein Purification

For expression of PFO/D4-GFP, the plasmid pRT10[22] was freshly transformed to expression competent cells (BL21 Star [DE3]pLysS One Shot Chemically Competent *E. coli*; Invitrogen, Carlsbad, CA, USA) resulting in *E. coli* BL21 PFO/D4-GFP. Transformed cells were grown on LB-Agar containing 100 μg/mL ampicillin for selection. A fresh overnight culture of *E. coli* BL21 PFO/D4-GFP in LB with 100 μg/mL ampicillin ($LB_{amp}$) was diluted in 1 L of $LB_{amp}$ with a final optical density ($OD_{600}$) of 0.05. Cells were cultured at 37°C overnight and PFO/D4-GFP expression was induced by IPTG and arabinose after 4 hours of incubation. Cells were purified and resuspended in PBS buffer containing 1 mM EDTA and protease inhibitors (Complete EDTA free, protease inhibitor cocktail tablets; Roche, Mannheim, Germany). *E. coli* BL21 PFO/D4-GFP cells were lysed by ultrasonication for 1 minute. The lysate was mixed with glutathion agarose/beads (Sigma-Aldrich Corp., Taufkirchen, Germany) and incubated overnight at 4°C under mild shaking.

Glutathion agarose/beads were harvested and washed three times with PBS buffer. Perfringolysin O/D4-GFP was eluated with 10 mM reduced glutathion and DTT was added. The PFO/D4-GFP eluate was enriched using a filter unit (Amicon Ultra 4, Centrifugal Filter Devices; Millipore Corp., Schwalbach, Germany). Protein concentration was determined using a Bradford assay (Quick Start Bradford, Dye; Bio-Rad, Hercules, CA, USA).

### Staining Procedure

For our staining protocols, we were guided by our experience with human Bruch's membrane samples.[10] We adapted the method to our murine samples and conducted prior to our final experiments multiple test series varying in time for unesterified cholesterol (UC) ethanol extraction and exposure for proteinase K, cholesterol esterase, and PFO/D4-GFP or filipin on chorioretinal sections and BrM wholemounts samples of aged ApoE$^{null}$ mice. We varied the ethanol extraction between 1 and 20 minutes and aimed for the minimum time, which ensured sufficient UC removal (artefact source). Proteinase K treatment on wholemount samples was varied between 1 and 10 minutes and aimed for improved dye penetration without significantly influencing the structural integrity of samples. Two different porcine cholesterol esterases were tested and the exposure was varied between 30 minutes and 5 hours at 37°C. The dyes were used in three concentrations and the exposure time varied between 30 minutes and 3 hours and overnight. Our final protocols that provided the best and repeatable results in our hands are listed as follows.

### Chorioretinal Sections

Slides with chorioretinal sections were removed from the freezer, air-dried for 1 hour, rehydrated for 15 minutes with PBS. Unesterified cholesterol was extracted by 70% ethanol for 5 minutes, followed by 2× rinse with PBS, and hydrolysis of EC by porcine cholesterol esterase (30 μg/mL; Fluka 29.0 U/mg; Sigma-Aldrich Corp., St. Louis, MO, USA) for 3 hours at 37°C. By applying PFO/D4-GFP (80 μg/mL) or filipin (250 μg/mL; Sigma-Aldrich Corp.) for 30 minutes, we detected the newly released UC in BrM. Light exposure was minimized during this and the following steps until dark field examination. After two short rinses, the samples were exposed to an AlexaFluor 488–labeled anti-GFP rabbit IgG antibody (dilution 1:200; Molecular Probes, Eugene, OR, USA) for 1 hour for an enhanced and stable fluorescent signal. Occasionally we contrast BrM with a counterstain (Isolectin IB4 AlexaFluor 568, 1:100, for 40 minutes; Molecular Probes) for capillary endothelial cells for better orientation. Slides were rinsed with PBS and coverslipped with a mounting medium (Mowiol 4-88; Carl Roth GmbH, Karlsruhe, Germany). Light exposure was minimized during handling.

### Controls

In our feasibility study, we used as a negative control the above-mentioned staining protocols on chorioretinal sections and wholemount samples, but after complete lipid extraction with Folch reagent (chloroform:methanol = 2:1) for 10 to 15 minutes. Additionally we used unstained section and wholemounts samples to evaluate the tissue autofluorescence and to set proper background fluorescence limits. A positive control was the detection of UC, which is abundantly present at each plasma membrane. The stains were applied directly onto the slides according to the above-mentioned protocol, but without ethanol extraction and cholesterol esterase treatment. Unesterified cholesterol was not detected anymore by both dyes after 5 minutes of 70% ethanol extraction.

### Wholemounts

We treated all BrM-choroid wholemounts with proteinase K (1 μg/mL in PBS; Sigma-Aldrich Corp.) for 5 minutes. After a 2× rinse with PBS, the samples were stained as described above but applied the stains for 1 hour. For consistent staining results and best dye penetration, all treatment steps were performed with free floating wholemounts. For maximum tissue flatness, all tissues were then mounted BrM down on silane pretreated coverslips.[10] After 2 minutes of drying, coverslips were inverted and mounted on glass microslides with mounting medium (Carl Roth GmbH). The BrM was now facing up for microscopy, still aligned to the coverslip's counterface.

### Imaging and Evaluation

Transmission electron microscopy samples were examined with an electron microscope (LEO 906E; Carl Zeiss Meditec, Oberkochen, Germany) with an automated image-capturing and processing system (DigiVision; Carl Zeiss Meditec).

All slides with chorioretinal sections were viewed with a fully automated inverse life science microscope (DMI 6000; Leica Microsystems) and fluorescence as well as differential interference contrast (DIC) images were captured with a high-sensitive digital camera (DFC350 FX; Leica Microsystems). For capturing fluorescence images different filter cubes (all from Leica Microsystems) depending on the used dye were used: for filipin, Leica A4 (excitation: BP 360/40, emission: BP 470/40); for PFO/D4-GFP-AlexaFluor 488, Leica L5 (excitation: BP 480/40, emission: BP 527/30); and for Isolectin IB4 AlexaFluor 568, Leica Y3 (excitation: BP 545/40, emission: BP 610/75). The microscope was operated and all image fluorescence was analyzed with a commercial software bundle (Leica Application Suite Advanced Fluorescence, version 2.3.0; Leica Microsystems).

The microscope was equipped with an automated x-y-z motor stage. From all wholemounts 8 to 10 image z-stages were recorded. Each z-stack covered 8 μm around the expected focus plane of BrM, which is in aged ApoE$^{null}$ mice just between 500- and 1000-nm thick. For optimal evaluation and fluorescence intensity measurements we selected the best focus plane after recording.

### Statistics

Our null hypothesis was that the overall fluorescent intensity of PFO/D4-GFP stained wholemounts is not associated with age and diet form in ApoE$^{null}$ mice. We performed *t*-tests with a statistical analysis tool (Biostat 2009 Professional, version 5.8.4.3; AnalystSoft, Inc., Alexandria, VA, USA). Statistical values ($P$) $\leq$ 0.05 (two-sided) were considered significant.

## Results

### Mouse Model

As expected, we found multiple lipid-derived vacuoles in thickened BrM and an advanced disarrangement of BrM laminar structure by TEM in aged ApoE$^{null}$ mice (Fig. 1). In contrast, the BrM structure in young animals was predominantly homogeneous with a regular pentalaminar structure (Fig. 1B). We observed only occasionally small lipid-derived vacuoles close to intercapillary pillars and no obvious BrM thickening.

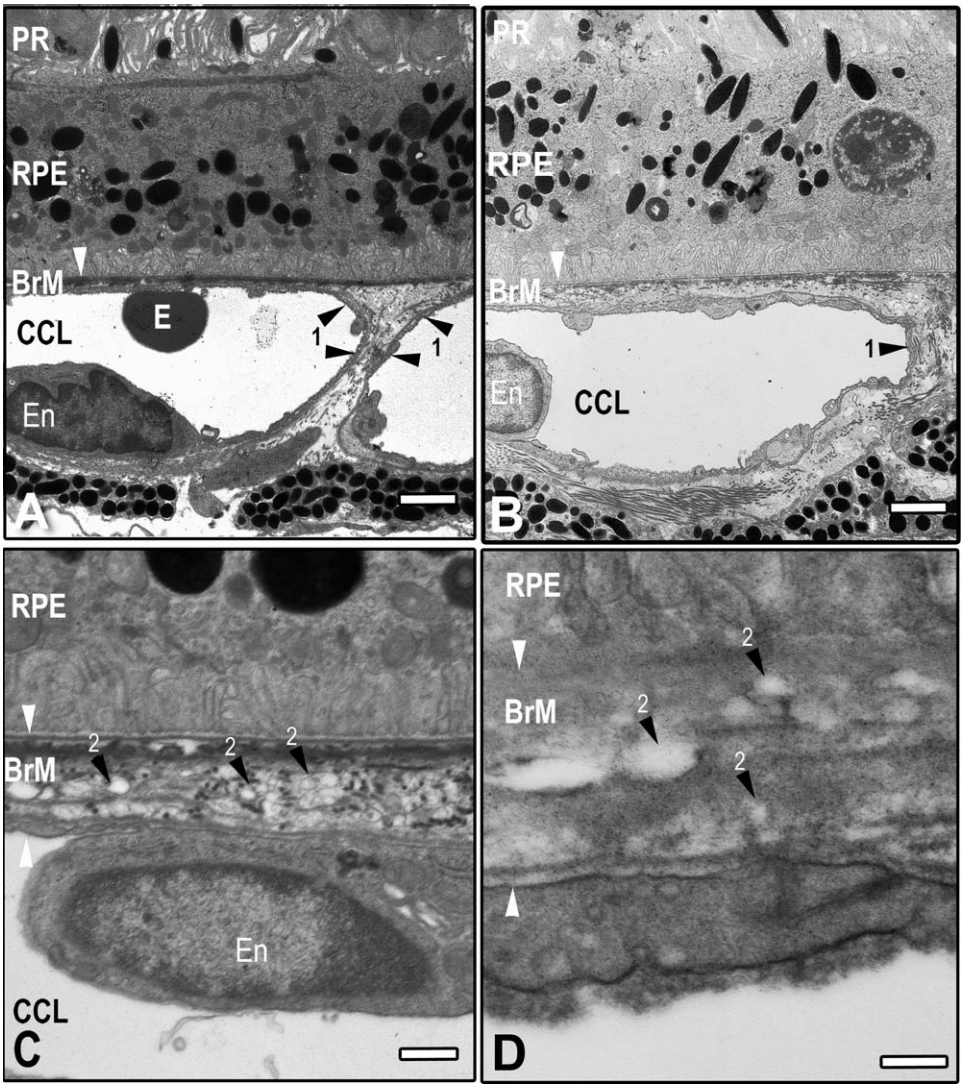


**Figure 1.** Transmission electron microscopy of murine Bruch's Membrane of young and aged ApoE$^{null}$ mice. *White arrow*: Bruch's membrane. BrM, Bruch's membrane; CCL, choriocapillary lumen; En, endothelial cell nucleus; PR, photoreceptors; E, erythrocyte. *Black arrow 1*: Choriocapillary pillar. *Black arrow 2*: translucent lipid-derived vesicles, all mice demonstrated here received only regular rodent chow, (**A**) ApoE$^{null}$ mouse, aged 3 months, BrM with regular structure, not thickened. *Scale bar*: 2 μm. (**B**) Thickened BrM with loss of regular pentalaminar structure of an 11-month-old ApoE$^{null}$ mouse. *Scale bar*: 2 μm. (**C**) ApoE$^{null}$ mouse, aged 11 months, with thickened BrM and exquisite preserved lipid vesicles. *Scale bar*: 200 nm. (**D**) ApoE$^{null}$ mouse, aged 11 months, with thickened BrM and lipid vesicles of varying sizes. *Scale bar*: 500 nm.

The high-cholesterol diet was not well tolerated by our aged ApoE$^{null}$ mice and caused several complications like massive weight gain (29.0 g ± 3.7 versus chow: 20.1 g ± 2.0, $P < 0.05$), skin rashes, and lethargy. After 6 weeks of a high-fat, high-cholesterol diet, we experienced six casualties in rapid succession. We decided to discontinue the diet for the remaining four animals and switched to regular chow again. As expected, we found in these mice abundant lipid-derived vacuoles by electron microscopy, but the difference to our aged mice on continuous regular chow was not apparent. Also, the direct measurement of EC content in BrM wholemounts with PFO/D4-GFP showed no significant difference between diet groups (see below). Since the high-cholesterol diet was very harmful to our aged mice and did not produce significantly more lipid deposits in BrM wholemounts, we decided to continue all following experiments with aged ApoE$^{null}$ mice without high-fat diets.

## Staining Results

Staining with both dyes for UC (positive control) in chorioretinal sections revealed a very intense but diffuse signal in the entire retina, RPE, and many areas in the choroid including BrM (not shown).

## EC in Chorioretinal Sections

Using our protocol for the detection of EC, we achieved a specific signal derived from BrM with filipin and PFO/D4-GFP (Figs. 2A, 2B, 3). We routinely amplified the PFO/D4-GFP signal with an AlexaFluor 488–labeled anti-GFP antibody, which made it even brighter, more extensive, and more stable.

Basically, both dyes stained identical structures (Figs. 2A, 2B). Complete lipid washout caused negative staining results for both dyes (Fig. 2C). The strong and stable fluorescence of PFO/D4-GFP/AlexaFluor 488 was suitable to visualize especial-

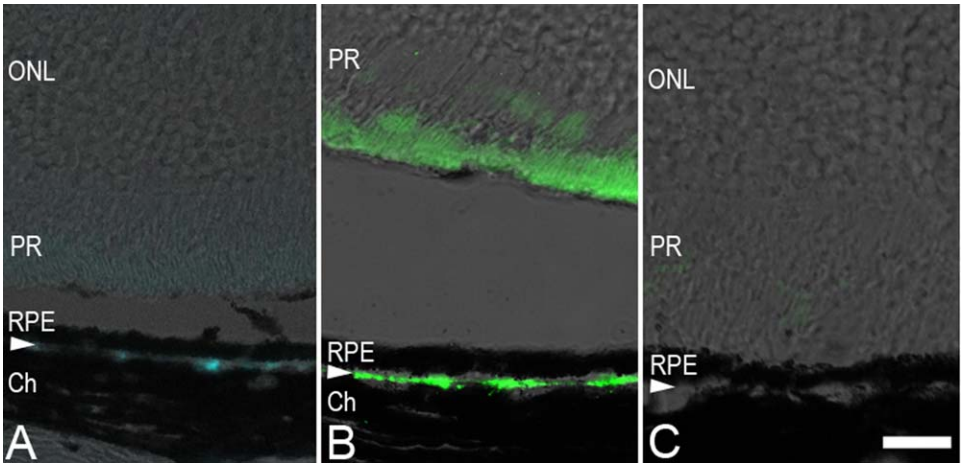


**Figure 2.** Esterified cholesterol in murine chorioretinal sections of aged ApoE$^{null}$ mice. Differential interference contrast images overlaid channels from wide-field fluorescence microscopy. (**A**) EC stained with filipin. (**B**) PFO/D4-GFP. (**C**) PFO/D4-GFP after complete lipid washout with Folch reagent (negative control). The PFO/D4-GFP signal was always amplified by a AlexaFluor–488 labeled anti-GFP antibody. ONL, outer nuclear layer. *White arrow*: BrM. Ch, choroid. *Scale bar*: 50 μm. (**A**) and (**B**) show a strong signal from the PR outer that vanished after complete lipid washout by Folch reagent in (**C**); EC is detected in BrM of 11-month-old ApoE$^{null}$ mice with (**A**) Filipin and (**B**) PFO/D4-GFP/AlexaFluor 488, but not in (**C**). In general, the signal from filipin is weaker and more focally located (advanced lipid accumulations in choriocapillary pillars). Relative to filipin, PFO/D4-GFP/AlexaFluor 488 signal is brighter, more extensive, and more stable. It revealed a continuous presence of EC in BrM. The signal is even increased by a slight tilting of BrM as a processing artifact. In (**A**, **B**) retina detached due to preparation artifacts; magnification: ×400.

ly small cholesterol quantities. Perfringolysin O/D4-GFP stained BrM continuously (Fig. 2B), in contrast to filipin that predominantly stained focally at the choriocapillary pillars where more lipids including cholesterol were trapped (Fig. 2A).

Intercapillary pillars' ultrastructure and count per area unit varies widely across an eye and across individual animals (Fig. 1). This fact highly limits an easy approach to a systematic analysis. For this reason, we decided to omit choriocapillary pillars from all our fluorescent measurements in wholemounts. Instead, we focused only on plain BrM over choriocapillary lumina.

By this approach, a highly standardized semiquantitative analysis of BrM-EC content was feasible. Nevertheless, artifacts must be considered and have to be omitted from analysis. A tilting of the delicate membrane was often detectable. It lowers the measurable fluorescence intensity significantly in these areas because part of the fluorescent structures were covered by RPE or by pigmented choroidal tissue. This artifact was less often detectable if retina and RPE were removed prior embedding, but this increased the preparation effort noticeably (Fig. 3). Nevertheless, this evaluation method was not as practical as a wholemount preparation to receive an overview over the entire Bruch's membrane at once.

## EC in BrM Wholemounts

Esterified cholesterol in murine BrM wholemounts was also detectable by both dyes. Filipin exhibited only faint spotted signals that bleached fast and precluded valid imaging (not shown). In contrast, we could detect and image for the first time reliably EC with PFO/D4-GFP in murine BrM wholemounts of aged ApoE$^{null}$ mice. The wholemount view revealed several structures. In untreated and unstained wholemounts

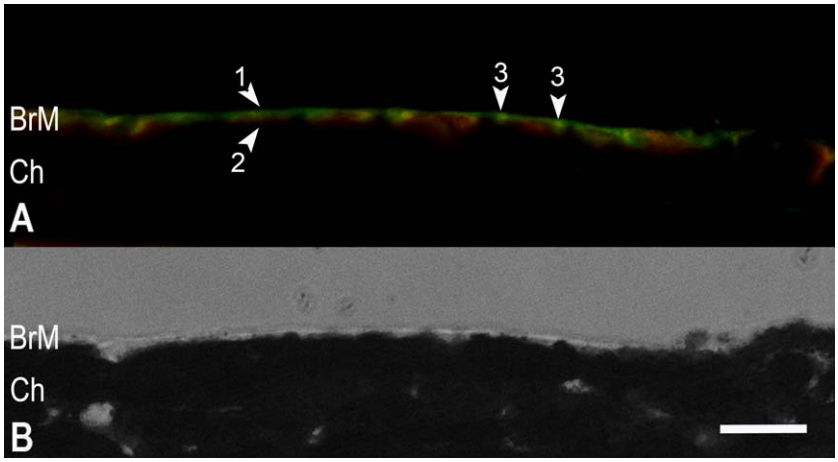


**Figure 3.** Staining pattern of PFO/D4-GFP in Bruch's membrane/choroid sections without RPE. Bruch's membrane/Ch complex of an 11-month-old ApoE$^{null}$ mouse. Removal of retina and the RPE reduced processing artifacts as tilting of BrM (**A**) PFO/D4-GFP/AlexaFluor 488 (*green*) stained for EC which is restricted to BrM (*arrow 1*), counterstain Isolectin IB4 AlexaFluor 568 (*red*) for capillary endothelial cells (*arrow 2*). Focal EC-rich protuberances of the right size and location for choriocapillary pillars (*green*, *arrow 3*) surround IB4-positive choriocapillary endothelial cells (*red*). (**B**) corresponding differential interference contrast image demonstrated clean removal of RPE. *Scale bar*: 20 μm.

Investigative Ophthalmology & Visual Science

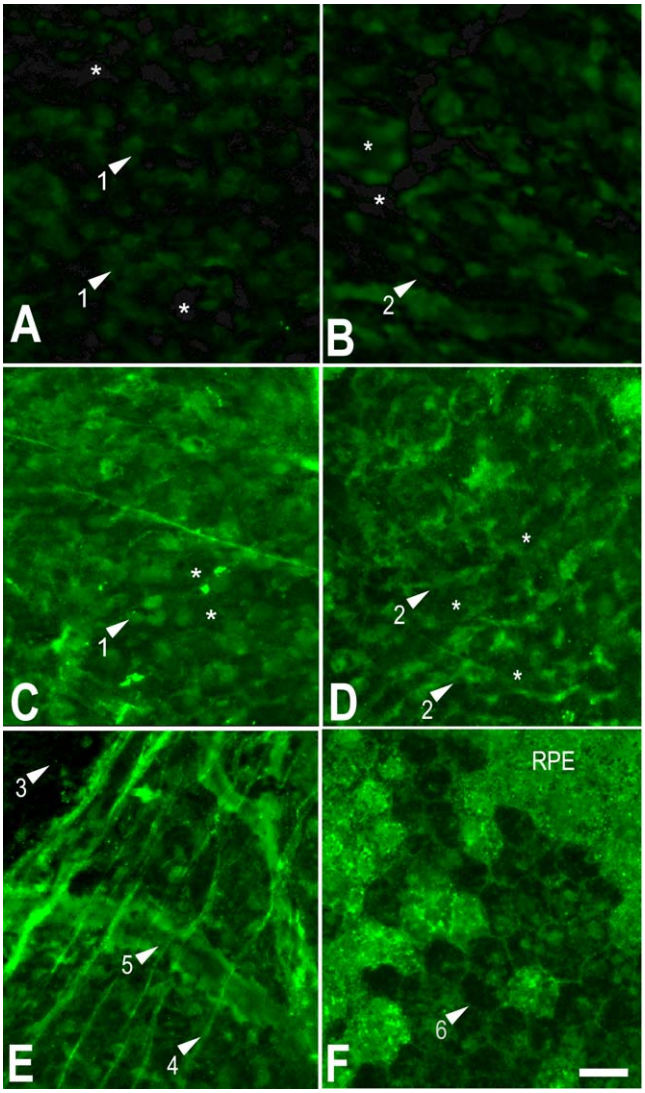


**Figure 4.** Esterified cholesterol detected with PFO/D4-GFP in wholemounts of murine Bruch's membrane/choroid of ApoE$^{null}$ mice. Cholesterol released from EC (see protocol) was detected with PFO/D4-GFP. The signal was amplified by a secondary anti-GFP antibody labeled with AlexaFluor 488. All images were taken using the same exposure parameters. *White scale bar:* 20 μm, applies to all panels. (**A**) untreated and unstained wholemount from an 11-month-old ApoE$^{null}$ mouse shows some autofluorescence from choriocapillary endothelial cell nuclei at the focus plane of BrM that impressed as round to oval, well-defined structures (*arrow 1*). Bruch's membrane with no interference from choriocapillary cells shows no autofluorescence (*asterisks*) at all. (**B**) Stained wholemount from a 3-month-old ApoE$^{null}$ mouse shows a slight patchy increase of EC (*upper asterisk*) next to areas with no increase of the dye signal (*lower asterisk*). Linear structures become apparent (*arrow 2*), representing an increased accumulation of EC in choriocapillary pillars. The overall staining effect is still low. (**C**, **D**) Intense staining of entire BrM of 11-month-old ApoE$^{null}$ mice. Bruch's membrane over choriocapillary endothelial cells (*arrow 1*) and choriocapillary pillars (*arrow 2*) stain also intensely and interfere with the actual BrM signal. Since the frequency of interfering choriocapillary endothelial cells and the density of choriocapillary pillars varies over a wholemount, we recommend for a standardized evaluation of BrM EC content multiple measurements of BrM over the choriocapillary lumen without interferences (*asterisks*). (**E**, **F**) Different artifacts must be considered that can influence standardized fluorescence measurements. These areas should be exempted from analysis: (3) A rip of Bruch's membrane shows that the fluorescent signal is located mainly in BrM itself. (4) wrinkling of BrM can focally increase the fluorescence signal. (5) Incomplete washout of serum lipids causes increased fluorescence from large choroidal vessels (shown) or from the choriocapillary network (not shown), very seldom intact RPE cells are left. (6) Remnants of RPE cell walls after incomplete removal.

from aged ApoE$^{null}$ mice, we found some autofluorescence from choriocapillary endothelial cell nuclei at the focus plane of BrM that impressed as round to oval, well-defined structures (Fig. 4A). Bruch's membranes with no interference from choriocapillary cells show no autofluorescence at all with our standard imaging setting (Fig. 4A). As a negative control we stained the wholemounts after a complete lipid washout by Folch reagent (not shown). The result corresponds to the appearance of an unstained wholemount (Fig. 4A). Stained wholemounts from young, 3-month-old ApoE$^{null}$ mice showed a slight patchy increase of EC next to areas with no increase of the fluorescence signal (Fig. 4B). Linear structures became apparent, representing an increased accumulation of EC in choriocapillary pillars. The overall staining effect was still low.

Age is a significant factor for lipid accumulation in murine BrM. We found that aged ApoE$^{null}$ mice (11–13 months) had on average 4.5 times more EC in BrM than 3-month-old ApoE$^{null}$ mice on chow feeding ($P < 0.001$, Fig. 5). An additional high-fat, high-cholesterol diet generated in aged animals an increase of EC of 13.8%, which was not statistically significant ($P = 0.39$, Fig. 5) but was accompanied by severe adverse events (see above).

In all aged ApoE$^{null}$ mice, we found an intense staining of the entire BrM (Figs. 4C–F). Choriocapillary pillars stained also intensely and interfered with the actual BrM signal. The number of intercapillary pillars per area unit varies widely across a wholemount. They are closer, packed close to the central optic nerve head compared with the wholemount periphery. That's why no general measurement of fluorescent intensity per area unit is applicable. For an appropriate standardized evaluation, we performed multiple measurements of plain BrM over the choriocapillary lumen omitting choriocapillary pillars, endothelial cell nuclei as well as the below-mentioned artefacts. We did not find a satisfactory segmentation mechanism to identify BrM-only areas automatically. We decided to take 10 images per wholemount and divided all images into three equal sectors from the bottom-left to the top-right corner. In each sector, a representative region of interest was marked with a free-form marking tool. This way we received an average of 30 measurements across an entire wholemount.

However, several artifacts must be considered. For instance, a rip of BrM by tissue processing (Fig. 4E ▶ 3) causes a typical non-fluorescent defect, which proves that the detected fluorescence originates mainly from BrM. Another artifact is seen if BrM is not completely flat. If mild, it showed a wrinkling of BrM with lines of compressed BrM with focally increased fluorescence (Fig. 4E ▶ 4). If advanced, there is no adequate focus for valid measurements. Incomplete washout of blood lipids caused also an increased fluorescence from large choroidal vessels (Fig. 4E ▶ 5) or from the choriocapillary network (not shown), which interfered with the BrM signal. Seldom intact RPE cells were left or remnants of RPE cell after incomplete removal that obscure BrM. Overall, the preparation and staining quality was high so that we could do valid measurements in over 90% of images.

## Discussion

Mouse models are essential to investigate biological pathways and pathological alterations, and to test new treatment

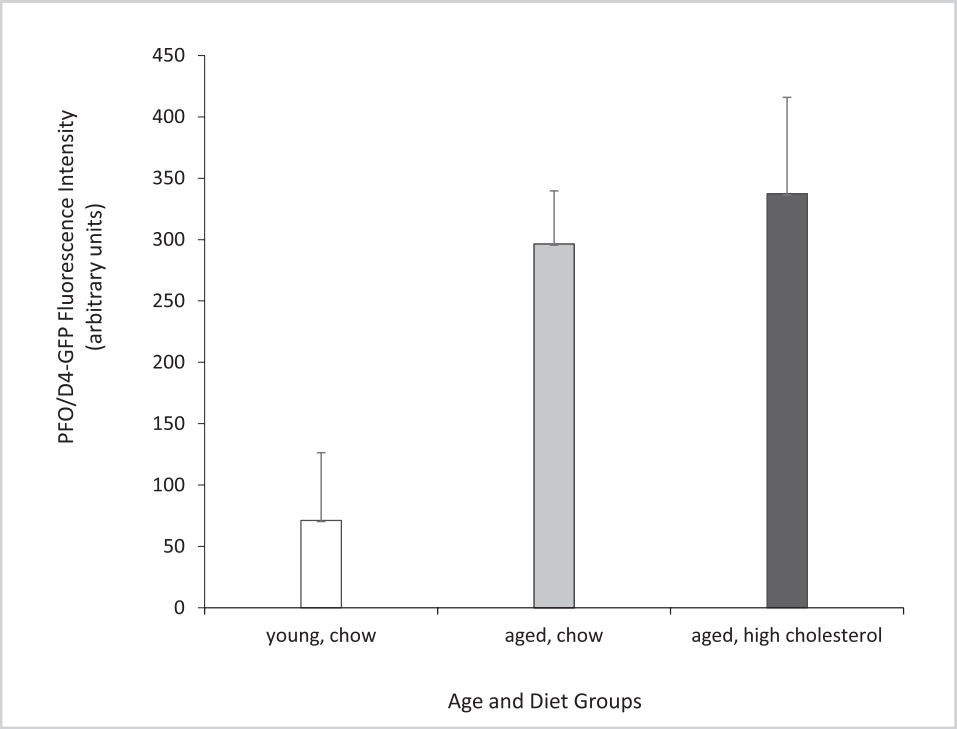


**Figure 5.** Age and diet forms on EC content in Bruch's membrane/choroid wholemounts of ApoE$^{null}$ mice. Three-month-old (young) and 11-month-old (aged) ApoE$^{null}$ mice were fed with standard chow. Ten aged animals were additionally fed with a high-fat, high-cholesterol diet for 6 weeks. After killing, BrM/choroid wholemounts were prepared and stained with PFO/D4-GFP for EC. Its fluorescence was measured as described in the text for semiquantitative analysis of BrM lipid content (mean ± SD). Advanced age was a significant factor to increase lipid deposits in BrM ($P < 0.001$). There was a tendency to a higher EC content in wholemounts of aged mice after consuming a high cholesterol diet. Nevertheless, the results were not significant ($P = 0.39$).

concepts. Even though there is not one mouse model that provides all features of AMD, there are many that provide partial aspects of the disease model.[23] Our research targets AMD-critical lipid accumulations in BrM, which we want to treat pharmacologically (Rudolf M, et al. *IOVS* 2010;51:ARVO E-Abstract 2984). With our tested novel cholesterol marker based on PFO, we developed a method to stain, for the first time, BrM-specific EC reliably in small quantities in sections and wholemounts of mice.

We produced the cholesterol marker PFO/D4-GFP via plasmid expression and compared it with the commercially available filipin for EC detection in murine BrM wholemounts and chorioretinal sections. We verified the presence of lipid accumulations in BrM of aged ApoE$^{null}$ mice with TEM, which is considered the gold standard. Relative to filipin, the PFO/D4-GFP signal is brighter, more intensive, and more stable. This difference is highly apparent if only small cholesterol quantities were present, which made it possible for the first time to image EC reliably in murine wholemounts. If larger quantities of cholesterol were present (e.g., if stained against UC), the difference between both dyes declined. Furthermore, PFO/D4-GFP can be combined with other standard processing features of immunohistochemistry to additionally enhance the signal strength or signal detectability. We routinely amplified the PFO/D4-GFP signal by a commercially available AlexaFluor 488–conjugated anti-GFP antibody. Others labeled a biotinylated PFO derivative even with colloidal gold to make cholesterol substructures by TEM detectable.[24]

Our results match the data, which show that PFO derivates/products are highly sensitive to detect cholesterol.[17,19,25] In most cases, it is used to detect small cholesterol-rich subunits in plasma membranes called lipid rafts.[17,18,26,27] Early approaches used PFO after enzymatic digestion and labeled the nontoxic cholesterol binding part with biotin for secondary detection.[3,18] A further development was the expression of the specific nontoxic D4 cholesterol binding side of PFO already bound to the visual marker GFP.[20,28,29] We also used such a construct in our study. To our knowledge, we used it first to specifically detect cholesteryl esters based on histochemical protocols for filipin by Kruth et al.[4] We adapted this protocol before for histology of the human eye and found EC specific for aged human BrM.[5,10] We can confirm this finding in our aged ApoE$^{null}$ mice. In humans, we know that the detected EC are associated with low-density lipoprotein particles that build up a hydrophobic diffusion barrier between the choriocapillaris and RPE.[2] These age-related lipid deposits are hallmarks of retinal aging[2,30] and are crucial for the development of oxidative stress and local inflammation, which trigger AMD based on environmental and genetic risk factors and are responsible for progression to advanced AMD stages.[31] Because PFO/D4-GFP can detect even small quantities of EC, we are now able to use mouse models to evaluate potential AMD treatment options targeting these crucial lipid deposits (Rudolf M, et al. *IOVS* 2010;51:ARVO E-Abstract 2984).

For our daily research, the reported approach of cholesterol detection has several advantages. For the first time, we can detect cholesterol directly and specifically even in small qualities in murine BrM wholemounts. It allows stable imaging and reliable evaluation in a much shorter time than with TEM. Stained BrM wholemounts provide at once a view over the entire BrM in contrast to the small area that can investigated in TEM samples.

We evaluated the reproducibility of our new staining results and analyzed factors influencing a systematic evaluation of

murine BrM EC content. We achieved a repeatedly excellent and stable preparation and staining quality for wholemounts. We had to learn to interpret interfering structures and artifacts with this new observation perspective. Most important are intercapillary pillars, which are structurally more complex than the regular pentalaminar BrM. They accumulated more lipids likely due to an elongated passage of metabolites from overlying RPE to the choriocapillary lumen. This effect is well-known from the histology of aged human BrM, where also the capitals of the choriocapillary pillars stain intensively with the neutral lipid stain oil red O.[10,30] Lipid-rich choriocapillary pillars might be important initiatory regions for early pathological changes and ignoring them in our analysis limits our method. Nevertheless, their high variability in size and fluorescence intensity per area unit conflicted an easy and highly standardized evaluation approach. We also found that fluorescence of endothelial cell nuclei measured in the z-stack right underneath the BrM level does not vary widely across an individual wholemounts or between animals so that is could provide a potential tool for data normalization.

We confirmed age as an important factor for lipid accumulation in murine BrM. Age is a major risk factor for AMD and for the accumulation of lipids in BrM.[30] But we did not find a significant influence of high-fat diet in aged animals as other studies did.[14,16] These studies did not detect lipids directly, but rather documented by TEM a progressive structural degeneration of BrM including presumably lipid-derived vesicles. Usually lipids are washed out during tissue processing for TEM. To preserve at least part of the lipids, the osmium-tannic acid-paraphenylenediamine method can be used, but was not published on murine BrM samples so far.[32–34] Nevertheless, we observed many severe adverse events under our high-fat, high-cholesterol diet so that we discontinued it. For this reason, and the nonsignificant increase of lipid depositions, we resigned the idea of even a less aggressive Western style, high-fat diet with lower cholesterol content. All together we experienced that, especially at a higher age ApoE$^{null}$, mice were quite sensitive to manipulations and had in our hands a natural limited lifetime with chow feeding of just 15 to 18 months.

## Acknowledgments

We thank Christine Örün for technical assistance.

Supported by the International Retinal Research Foundation (USA), Jackstädt-Stiftung (Germany), and the AMD-Förderpreis der Deutschen Ophthalmologischen Gesellschaft 2009 (Germany).

The authors alone are responsible for the content and writing of the paper.

Disclosure: **M. Rudolf**, None; **A. Mohi**, None; **M.C. Dettbarn**, None; Y. Miura, None; **Z. Aherrahrou**, None; **M. Ranjbar**, None; **B. Mutus**, None; **J.K.M. Knobloch**, None

## References

1. Kruth HS. The fate of lipoprotein cholesterol entering the arterial wall. *Curr Opin Lipidol*. 1997;8:246–252.
2. Curcio CA, Johnson M, Rudolf M, Huang JD. The oil spill in ageing Bruch membrane. *Br J Ophthalmol*. 2011;95:1638–1645.
3. Reid PC, Sakashita N, Sugii S, et al. A novel cholesterol stain reveals early neuronal cholesterol accumulation in the Niemann-Pick type C1 mouse brain. *J Lipid Res*. 2004;45:582–591.
4. Kruth HS, Cupp JE, Khan MA. Method for detection and isolation of cholesteryl ester-containing "foam" cells using flow cytometry. *Cytometry*. 1987;8:146–152.
5. Curcio CA, Millican CL, Bailey T, Kruth HS. Accumulation of cholesterol with age in human Bruch's membrane. *Invest Ophthalmol Vis Sci*. 2001;42:265–274.
6. Castanho MA, Coutinho A, Prieto MJ. Absorption and fluorescence spectra of polyene antibiotics in the presence of cholesterol. *J Biol Chem*. 1992;267:204–209.
7. Gimpl G, Gehrig-Burger K. Cholesterol reporter molecules. *Biosci Rep*. 2007;27:335–358.
8. Wang L, Li CM, Rudolf M, et al. Lipoprotein particles of intraocular origin in human Bruch membrane: an unusual lipid profile. *Invest Ophthalmol Vis Sci*. 2009;50:870–877.
9. Li CM, Chung BH, Presley JB, et al. Lipoprotein-like particles and cholesteryl esters in human Bruch's membrane: initial characterization. *Invest Ophthalmol Vis Sci*. 2005;46:2576–2586.
10. Rudolf M, Curcio CA. Esterified cholesterol is highly localized to Bruch's membrane, as revealed by lipid histochemistry in wholemounts of human choroid. *J Histochem Cytochem*. 2009;57:731–739.
11. Ramrattan RS, van der Schaft TL, Mooy CM, et al. Morphometric analysis of Bruch's membrane, the choriocapillaris, and the choroid in aging. *Invest Ophthalmol Vis Sci*. 1994;35:2857–2864.
12. Bretillon L, Acar N, Seeliger MW, et al. ApoB100, LDLR$^{-/-}$ mice exhibit reduced electroretinographic response and cholesteryl esters deposits in the retina. *Invest Ophthalmol Vis Sci*. 2008;49:1307–1314.
13. Dithmar S, Curcio CA, Le NA, Brown S, Grossniklaus HE. Ultrastructural changes in Bruch's membrane of apolipoprotein E-deficient mice. *Invest Ophthalmol Vis Sci*. 2000;41:2035–2042.
14. Dithmar S, Sharara NA, Curcio CA, et al. Murine high-fat diet and laser photochemical model of basal deposits in Bruch membrane. *Arch Ophthalmol*. 2001;119:1643–169.
15. Rudolf M, Ivandic B, Winkler B, et al. Increased expression of vascular endothelial growth factor associated with accumulation of lipids in Bruch's membrane of LDL receptor knockout mice. *Br J Ophthalmol*. 2005;89:1627–1630.
16. Schmidt-Erfurth U, Rudolf M, Funk M, et al. Ultrastructural changes in a murine model of graded Bruch membrane lipoidal degeneration and corresponding VEGF164 detection. *Invest Ophthalmol Vis Sci*. 2008;49:390–398.
17. Tweten RK. Cholesterol-dependent cytolysins, a family of versatile pore-forming toxins. *Infect Immun*. 2005;73:6199–6209.
18. Iwamoto M, Morita I, Fukuda M, Murota S Ando S, Ohno-Iwashita Y. A biotinylated perfringolysin O derivative: a new probe for detection of cell surface cholesterol. *Biochim Biophys Acta*. 1997;1327:222–230.
19. Soltani CE, Hotze EM, Johnson AE, Tweten RK. Structural elements of the cholesterol-dependent cytolysins that are responsible for their cholesterol-sensitive membrane interactions. *Proc Natl Acad Sci U S A*. 2007;104:20226–2031.
20. Miersch S, Espey MG, Chaube R, et al. Plasma membrane cholesterol content affects nitric oxide diffusion dynamics and signaling. *J Biol Chem*. 2008;283:18513–1821.
21. Vogt SD, Curcio CA, Wang L, et al. Retinal pigment epithelial expression of complement regulator CD46 is altered early in the course of geographic atrophy. *Exp Eye Res*. 2011;93:413–423.
22. Mutus B. Plasmid pRT10. Available at: https://www.lablife.org/g?a=seqa&id=vdb_g2.f392707aa9473fdf68d26da36e19b0a5d9705215_sequence_8bf487f86350fafe4335358d132f344bc3b33fe8_10. Accessed December 1, 2013.
23. Zeiss CJ. Animals as models of age-related macular degeneration: an imperfect measure of the truth. *Vet Pathol*. 2010;47:396–413.

24. Mobius W, Ohno-Iwashita Y, van Donselaar EG, et al. Immunoelectron microscopic localization of cholesterol using biotinylated and non-cytolytic perfringolysin O. *J Histochem Cytochem*. 2002;50:43–55.
25. Ramachandran R, Heuck AP, Tweten RK, Johnson AE. Structural insights into the membrane-anchoring mechanism of a cholesterol-dependent cytolysin. *Nat Struct Biol*. 2002;9: 823–827.
26. Das A, Goldstein JL, Anderson DD, Brown MS, Radhakrishnan A. Use of mutant 125I-perfringolysin O to probe transport and organization of cholesterol in membranes of animal cells. *Proc Natl Acad Sci U S A*. 2013;110:10580–10585.
27. Waheed AA, Shimada Y, Heijnen HF, et al. Selective binding of perfringolysin O derivative to cholesterol-rich membrane microdomains (rafts). *Proc Natl Acad Sci U S A*. 2001;98: 4926–4931.
28. Ohno-Iwashita Y, Shimada Y, Waheed AA, et al. Perfringolysin O, a cholesterol-binding cytolysin, as a probe for lipid rafts. *Anaerobe*. 2004;10:125–134.
29. Shimada Y, Maruya M, Iwashita S, Ohno-Iwashita Y. The C-terminal domain of perfringolysin O is an essential cholesterol-binding unit targeting to cholesterol-rich microdomains. *Eur J Biochem*. 2002;269:6195–6203.
30. Pauleikhoff D, Harper CA, Marshall J, Bird AC. Aging changes in Bruch's membrane. A histochemical and morphologic study. *Ophthalmology*. 1990;97:171–178.
31. Zarbin MA. Current concepts in the pathogenesis of age-related macular degeneration. *Arch Ophthalmol*. 2004;122: 598–614.
32. Johnson M, Dabholkar A, Huang JD, Presley JB, Chimento MF, Curcio CA. Comparison of morphology of human macular and peripheral Bruch's membrane in older eyes. *Curr Eye Res*. 2007;32:791–799.
33. Rudolf M, Clark ME, Chimento MF, et al. Prevalence and morphology of druse types in the macula and periphery of eyes with age-related maculopathy. *Invest Ophthalmol Vis Sci*. 2008;49:1200–1209.
34. Guyton JR, Klemp KF. The lipid-rich core region of human atherosclerotic fibrous plaques. Prevalence of small lipid droplets and vesicles by electron microscopy. *Am J Pathol*. 1989;134:705–717.

Investigative Ophthalmology & Visual Science